ADVANCED FUNCTIONAL MATERIALS
www.afm-journal.de

Materials Views
www.MaterialsViews.com

Highly Porous and Preferentially Oriented {100} Platinum Nanowires and Thin Films

*Alexandre Ponrouch, Sébastien Garbarino, Erwan Bertin, Carmen Andrei, Gianluigi A. Botton, and Daniel Guay**

Highly {100} oriented Pt deposits were prepared by electrodeposition from a 10 mM HCl, 100 mM KCl and $Na_2PtCl_6.xH_2O$ electrolyte. The deposits were prepared in the form of thin films and array of nanowires. A qualitative assessment of the proportion of {100} oriented Pt surfaces was obtained through X-ray diffraction measurements and cyclic voltammetry in 0.5 M H_2SO_4. The effect of the deposition potential, E_{dep}, temperature of the electrolyte, T_{dep}, platinum salt concentration [$Na_2PtCl_6.xH_2O$], and nature of the substrate were investigated. It was shown that the proportion of {100} oriented Pt surfaces reaches a maximum for $E_{dep} = -0.35$ V vs SCE. Moreover, this proportion increases steadily as T_{dep} and [$Na_2PtCl_6.xH_2O$] are decreased from 75 to 25 °C and from 2.5 to 0.25 mM, respectively. Scanning electron microscopy and high-resolution transmission electron microscopy micrographs indicate that the more oriented samples are made of pine tree-like structures that are effectively single crystals, and that the growth facets appear to be close to the {001} plane. This observation also clearly indicates that the plane exposed during the CV experiment is also {001}. As suggested by these micrographs, the films and nanowires are highly porous and roughness factors as large as 1000 were obtained on highly {100} oriented Pt nanowires. The predominance of {100} facets is attributed to their energetically favoured growth in the presence of hydrogen, and is shown to be significantly enhanced when the mass transport of Pt^{4+} is limited. Due to the predominance of {100} facets, the normalized electrocatalytic activity ($\mu A\ cm^{-2}_{Pt}$) for the electro-oxidation of hydrazine and ammonia is higher than non-oriented polycrystalline Pt by a factor of 4 and 2.7, respectively.

1. Introduction

The electrochemical oxidation of ammonia and hydrazine has been studied for many years. This interest stems from the fact that ammonia oxidation is important in the fabrication of electrochemical sensors for water and air analyses. In addition, ammonia is a common water pollutant in industrial wastewaters and in continental waters. Therefore, the development of an electrochemical method to convert ammonia into nitrogen would open up new possibilities in environmental electrochemistry. Likewise, hydrazine is important in numerous industrial applications, including metal plating and protection against corrosion to control concentrations of dissolved oxygen. It is also used in various rocket fuels and as a component in explosives. Hydrazine is highly toxic and its electrochemical detection is also of significant interest. Finally, the most recent developments in low-temperature fuel cell technology have shown nitrogen hydrides, ammonia, and hydrazine to be suitable candidates in the race for commercial, high-performance, portable fuel cells.[1]

Several studies have been devoted to the electro-oxidation of ammonia and hydrazine on polycrystalline substrates. More recently, studies of ammonia and hydrazine oxidation on single-crystal metal surfaces have been reported, providing evidence that the electro-oxidation process of these small nitrogen hydride molecules is structure-sensitive.[2–8] For example, in acidic solution, Nishihara et al[2] found that hydrazine adsorbs more readily on Pt (100) steps than on Pt (111) terraces. While Alvarez-Ruiz et al[4] showed that the basal planes of platinum and rhodium are much more active for hydrazine oxidation than the corresponding gold surfaces, they also showed that the (100) plane was one of the most active planes for all three metals. In alkaline media, the electrocatalytic activity of basal planes increases in the order Pt(110)>Pt(100)>Pt(111).[5] Likewise, in alkaline media, the electro-oxidation of ammonia on Pt occurs almost exclusively on surface sites with (100) symmetry.[6–8]

Therefore, from a practical viewpoint, it would be highly desirable to prepare Pt electrodes that could exhibit both a high electrochemically active surface area and a preferentially-oriented {100} surface structure. In the early 1970s, several papers from Arvia's group described an electrochemical

Dr. A. Ponrouch, Dr. S. Garbarino, E. Bertin, Prof. D. Guay
INRS-Énergie, Matériaux et Télécommunications
1650 Blvd. Lionel-Boulet, C.P. 1020, Varennes
QC J3X 1S2 Canada
E-mail: guay@emt.inrs.ca
Dr. C. Andrei, Prof. G. A. Botton
Department of Materials Science and Engineering
Brockhouse Institute for Material Research
Canadian Centre for Electron Microscopy
McMaster University
Hamilton, ON L8S 4L7 Canada

DOI: 10.1002/adfm.201200381

procedure to obtain Pt electrode surfaces with preferred orientations from bulk polycrystalline platinum. The procedure used to achieve this is based on the use of repetitive potential sweeps at high frequency under carefully-selected potential perturbation conditions.[9–11] Under the right conditions, the formation of preferentially-oriented {100} surfaces was achieved, but the roughness factor was low and does not exceed R = 3.[9] Under these conditions, while the intrinsic electrocatalytic activity (expressed as current per Pt surface atom) for the electro-oxidation of nitrogen hydrides might be high, the overall electrocatalytic activity (expressed as current per geometric surface area) will remain low as a result of the low roughness factor.

Several groups have focused on the use of preferentially-oriented {100} platinum particles to combine both a high intrinsic electrocatalytic activity and high electrochemically active surface area.[12] These particles consist of Pt cubic nanoparticles synthesized in the form of colloidal platinum, using a capping agent (sodium polyacrylate) and hydrogen gas as a reducing agent.[13] According to high-resolution transmission electron microscopy, these nanoparticles show flat surfaces with {100} facets, and the distances between the adjacent lattice fringes is the interplanar distance of Pt {200}.[14] Pt nanoparticles prepared using the same method elsewhere have been shown to exhibit characteristic hydrogen adsorption/desorption peaks,[12,15–19] CO-stripping peaks,[15,17] as well as the characteristic response of irreversibly-adsorbed germanium on (100) sites of platinum.[18,19] These oriented nanoparticles show higher current densities for the electro-oxidation of ammonia in alkaline media than polycrystalline Pt nanoparticles.[12]

Colloidal methods using organic ligand stabilizers are one of the most commonly used methods to make shape-controlled particles. However, the organic ligand shells can be difficult to remove. Various methods have been devised for cleaning the nanoparticles, such as heating in different atmospheres or submitting the nanoparticle to electrochemical decontamination by surface oxidation. However, these methods could produce a change in the surface structure. It was shown that modification of the surface structure may be limited if electrochemical decontamination is performed under the right conditions, however, residual surfactant molecules were still present, causing an incomplete deposition of the Pt nanoparticles (floating) on the surface of the substrate.[20] From a more pragmatic point of view, the preparation of an electrode from an assembly of such nanoparticles is also challenging.

In contrast, electrochemical deposition is a fast, simple method which can produce three-dimensional particles directly attached onto a substrate or support. It is a one-step technique that requires no additional purification step, and its implementation is straightforward. It also has the added benefit of being applicable to substrates of different natures and geometric shapes. Moreover, it was shown recently that electrodeposition might be used to prepare metallic particles of various shapes. For example, it was demonstrated that granular Cr nanoparticles or hexagonal microrods could be obtained depending on the deposition conditions,[21] and the synthesis of tetrahexahedral Pd nanocrystals with high Miller Index facets was demonstrated using a pulse electrodeposition method.[22] Likewise, it was shown recently that Pt nanowire with preferentially-oriented {100} surfaces could be prepared through template-assisted deposition, using an anodic aluminum oxide membrane.[23]

In this study, highly porous Pt deposits in the form of thin films and nanowires were prepared with a large proportion of preferentially-oriented {100} surfaces. A systematic study of the deposition conditions affecting the proportion of those preferentially-oriented {100} surfaces was conducted. The benefits of using a porous Pt-based electrode with a large fraction of {100} surfaces are demonstrated by investigating the electro-oxidation of hydrazine in sulphuric acid and of ammonia in alkaline electrolyte.

2. Results and Discussion

2.1. Electrochemical Characterization

Cyclic voltammetry (CV) is a surface-sensitive technique which enables in situ qualitative estimation of the amount of different sites present on a platinum surface. This is because the hydrogen sorption processes are very sensitive to the surface structure. Thus, CVs of Pt electrodes prepared under different deposition parameters are noted in **Figure 1**. In all cases, the upper potential limit was restricted to 0.80 V to avoid any crystallographic surface change.[20] In the forward sweep, three main anodic peaks are observed at *ca.* 0.12 (h_1), 0.26 (h_2) and 0.37V (h_3). As discussed elsewhere, the presence of the aforementioned hydrogen desorption peaks may be used as a fingerprint for the various crystallographic components of the platinum surfaces. Thus, based on the literature, the anodic peaks h_1, h_2 and h_3 are attributed to hydrogen desorption from (110) sites, (100) step sites and (100) terrace sites respectively.[19,24,25] As seen in Figure 1, the maximum peak current of these various features varies with the deposition conditions.

In the past, the h_2/h_1 peak current ratio was used to provide a qualitative assessment of the proportion of (100) surface sites[26,27] on Pt samples. However, more recent studies have shown that a

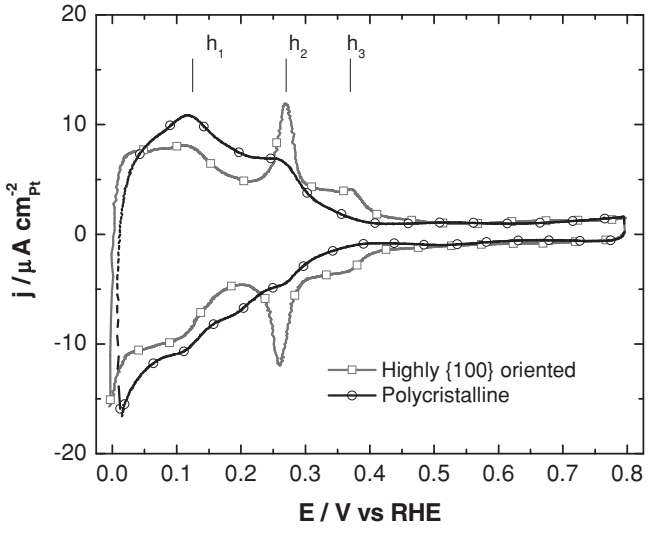

Figure 1. Cyclic voltammetric curves (5 mVs^{-1}) of polycrystalline and highly-oriented {100} Pt deposits in 0.5 M H_2SO_4. The positive limit of the scan was restricted to +0.80V.

quantitative analysis of the different surface sites on platinum samples may be performed by using specific site-probe reactions and deconvolution of the hydrogen desorption peaks.[18,19,24] To evaluate these protocols, the authors have relied on Pt nanoparticles of different sizes and shapes.[18] A comparison between the h_2/h_1 peak current ratio measured on their CVs and the fractions of (111) and (100) sites determined from their deconvolution of the hydrogen desorption region and site-specific adsorption of Bi, Te, and Ge is shown in Figure S1. Based on this analysis, one can roughly estimate the amount of (100) surface sites on Pt samples from an inspection of the CVs. The h_2/h_1 peak current ratios observed in the two CVs in Figure 1 are 0.6 and 1.6, which correspond to a proportion of (100) surface sites of *ca*. 20 and 65%, respectively. In Figure 1, it is also interesting to note the high h_2/h_1 peak current ratio indicative of a large proportion of (100) surface sites is also accompanied by a marked contribution at *ca*. 0.37V (h_3) that is attributed to wide (100) terraces.[19] Both results are consistent and are indicative that the amount of (100) surface sites (either step sites or terraces) may be adjusted through careful selection of the deposition conditions.

It is widely known from the literature that (100) surface sites are not stable upon potential cycling up to 1.50V, and that oxide formation at the surface of the electrode causes the disruption of the ordered (100) domains.[28] Thus, to further emphasize that (100) sites are present at the surface of Pt deposits, a series of 300 CVs were performed between 0.05 and 1.50V (50 mVs^{-1} in 0.5 M H_2SO_4). The CV recorded between 0.0 and 0.8V following that procedure (see **Figure 2**) is radically different when compared to the previous one. The decrease of the voltammetric peak h_3 at *ca*. 0.37V, and the significant decrease of the h_2/h_1 ratio, reveals the loss of the wide (100) surface domains and a lower proportion of (100) exposed step sites, respectively. At the same time, there is a significant decrease of the current in the double-layer region (expressed as $mA.cm^{-2}_{geometric}$), indicating that Pt dissolution (and reorganization) has taken place. Similar behaviour (not shown) was observed for all Pt films which exhibited a large fraction of (100) surface sites and surface domains in the as-prepared state.

The fact that the h_2/h_1 peak current ratio could be irreversibly modified by increasing the positive potential limit of the scan is also a clear indication that current associated with peak h_2 is not related to the oxidation of a solution impurity that could have been deposited on the surface of the electrode during the preceding cathodic sweep.

The amount of (100) surface sites depends on a delicate balance between several electrodeposition parameters. In an upcoming section, the influence of the deposition parameters on the structural and morphological properties of electrodeposited Pt will be investigated, with the objective of identifying the conditions that give rise to Pt deposits showing the highest proportion of (100) surface sites. However, prior to that, it will be shown that these films exhibit a distinctive structural characteristic which may be recognized through their XRD patterns.

2.2. Structural Characterization

XRD patterns were recorded to characterize the bulk crystallographic structure of the Pt deposits. Typical XRD patterns of polycrystalline and highly-oriented {100} Pt deposits are shown in **Figure 3**. In all cases, the X-ray diffraction patterns depict the five diffraction peaks characteristic of the face-centered cubic (FCC) structure of platinum, with peaks at 2θ = 39.76°, 46.24°, 67.46°, 81.29° and 85.72°, corresponding to the crystallographic planes (111), (200), (220), (311) and (222), respectively. As seen in Figure 3, the XRD peaks of highly-oriented {100} Pt deposits are narrower than polycrystalline Pt, indicating an increase of the crystallite size. This is consistent with the TEM micrographs that are going to show that the former deposits are made of a collection of "single crystals" whose dimensions exceed 25–30 nm.

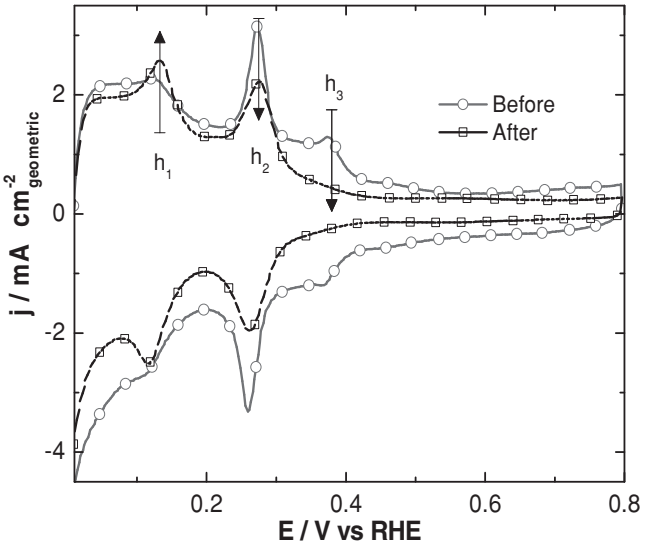

Figure 2. Cyclic voltammetric curves ($5mVs^{-1}$, 0.5 M H_2SO_4) of as-deposited highly-oriented {100} Pt deposits and after it was cycled up to 1.50 V (300 cycles at $50mVs^{-1}$).

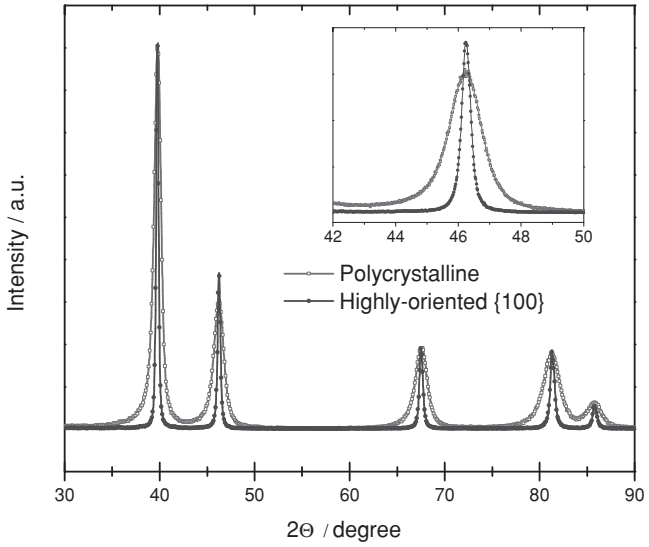

Figure 3. XRD patterns of polycrystalline and highly-oriented {100} Pt deposits. The XRD patterns were normalized with respect to the intensity of the (220) peak of Pt at 2θ = 67.5°.

The XRD patterns of the various deposits were first normalized to facilitate comparison between them. However, in some cases (not shown), the characteristic diffraction peaks of the Ti substrate were also observed in the XRD pattern. The position of the most prominent diffraction peak of Ti ($2\theta = 40.17°$, corresponding to the (101) diffraction peak) is superimposed on the (111) peak of Pt ($2\theta = 39.76°$). In most cases, this contribution is small; but a detailed analysis of the peak shape clearly indicates that the (111) peak of Pt presents a small asymmetry not observed on the other diffraction peaks of the same deposit. Therefore, there is some overlap between the (111) peak of Pt and the (101) peak of Ti, and using the integrated intensity (or the maximum intensity) of the (111) peak of Pt to normalize the various XRD patterns might introduce a systematic error. Instead, the maximum intensity of the (220) peak of Pt was chosen to normalize the XRD patterns, since the Ti substrate does not have any diffraction peaks in that region.

The XRD patterns shown in Figure 3 have been normalized with respect to the (220) maximum peak intensity. As a result, the maximum peak intensities of all peaks of a highly {100} oriented Pt deposit (corresponding to the open square CV of Figure 1) are identical (within 3–5%) to those observed on the XRD patterns of a non-oriented polycrystalline Pt deposit (corresponding to the open circle of Figure 1), except for the (200) maximum peak intensity, which shows a marked difference (*ca.* 20%) between both types of deposits (see the inset to Figure 3). An identical conclusion is reached when the integrated intensity (instead of the maximum intensity) of the (220) peak of Pt is used in the normalization procedure. The fact that the relative intensity of the (200) peak varies is a clear indication that a preferential orientation along the {100} axis exists in some of the Pt deposits.

The evolution of the h_2/h_1 ratio, which is a measure of the surface orientation as determined by electrochemical measurements, with respect to $I_{max}(200)/I_{max}(220)$, which is defined as the ratio between the maximum peak intensity of the (200) and (220) peak of a deposit and is related to the bulk orientation of the deposition as determined by XRD measurements, is presented in **Figure 4**. For as-prepared samples, there is a quasi-linear relationship between both values. This linear relationship is observed for every sample, regardless of the deposition parameters and the nature of the deposits (TF or NW). Since XRD is a bulk-sensitive technique, it is straightforward to conclude that the preferential crystallographic orientation evidenced through the use of CV is also found in the bulk of the deposit. In the following section, XRD data will be used to assess the effects of the various deposition conditions on the surface orientation of the Pt deposit.

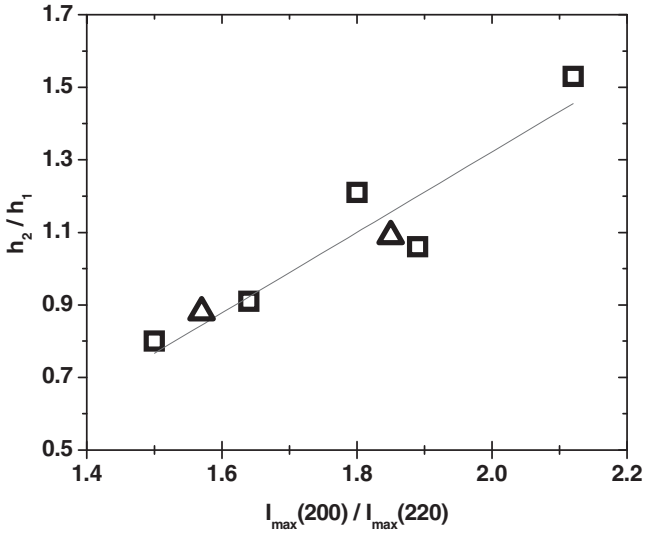

Figure 4. Variation of h_2/h_1 with respect to $I_{max}(200)/I_{max}(220)$. The h_2/h_1 ratio is determined from cyclic voltammetric curves ($5 mVs^{-1}$) in 0.5M H_2SO_4, while the $I_{max}(200)/I_{max}(220)$ ratio is defined as the ratio between the maximum peak intensity of the (200) and (220) XRD peak of the same deposit. Data in this figure was taken from the XRD patterns of both Pt TFs (open triangles) and Pt NWs (open squares).

2.3. Effects of the Deposition Conditions

A series of Pt deposits were prepared by varying (i) the deposition potential, E_{dep}, (ii) the temperature of the electrolyte, T_{dep}, (iii) the presence of an AAO membrane at the surface of the Ti substrate, (iv) the Pt salt concentration, and (v) the nature of the substrate. In each case, the XRD patterns were recorded. **Figure 5** outlines how the $I_{max}(200)/I_{max}(220)$ ratio varies with the deposition conditions

(i) Effect of E_{dep}: In this series of measurements, an AAO membrane was held firmly in front of the Ti substrate. As shown elsewhere,[23,29,30,31] this led to the formation of an array of Pt nanowires on the surface of the substrate. All deposition parameters were kept constant (1 mM of Na_2PtCl_6; 100 mM

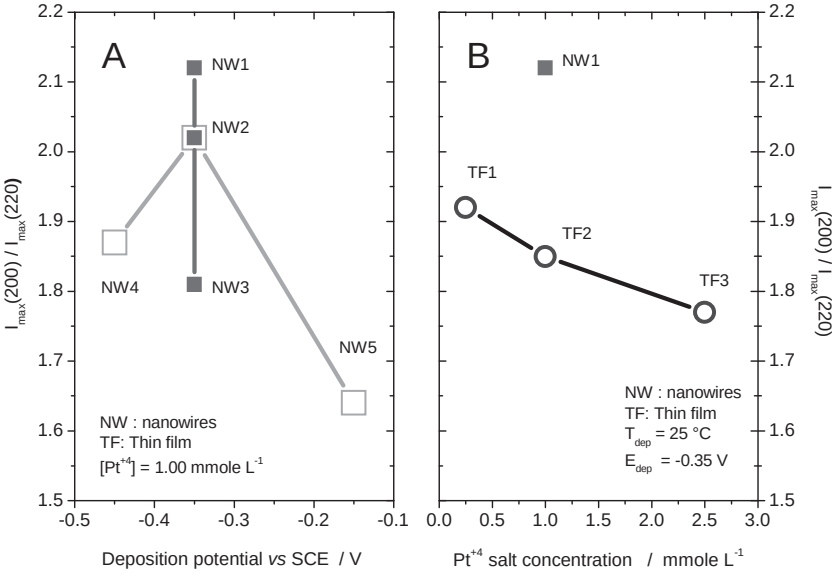

Figure 5. Variation of the $I_{max}(200)/I_{max}(220)$ ratio with respect to (A) the deposition potential and (B) the Pt^{4+} salt concentration. A detailed description of the deposition conditions of the various samples is provided in the study.

KCl; 10 mM HCl; T_{dep} = 50 °C), except for the deposition potential, E_{dep}, that was varied from –0.15, –0.35 and –0.45V for samples NW5, NW2 and NW4, respectively. As seen in Figure 5A, the $I_{max}(200)/I_{max}(220)$ ratio increases from 1.64 ± 0.02 to 2.02 ± 0.02 as E_{dep} is decreased from –0.15 to –0.35V. Pt nanowires prepared at more negative potential (E_{dep} = –0.45V) exhibit a lower $I_{max}(200)/I_{max}(220)$ ratio (1.87 ± 0.02).

It is worth noting that, according to the JCPDS card 004-0802, the (200)/(220) integrated intensity ratio of polycrystalline Pt is 1.7. As seen in Figure 5A, Pt deposition at potentials more positive than the reversible hydrogen potential leads to the deposition of Pt film with no preferential orientation. However, lowering the potential to values more negative than the reversible hydrogen potential significantly increases the $I_{max}(200)/I_{max}(220)$ ratio which, according to the results in Figure 5, indicates that a significant proportion of (100) sites exist at the electrode surface. Decreasing the potential to even more negative values decreases the $I_{max}(200)/I_{max}(220)$ ratio, and thus, there is an optimal value of the electrode potential for the deposition of highly {100} oriented Pt.

(ii) Effect of T_{dep}: In this series of measurements, an AAO membrane was held firmly in front of the Ti substrate and Pt nanowires were formed. All deposition parameters were kept constant (1 mM of Na_2PtCl_6; 100 mM KCl; 10 mM HCl; E_{dep} = –0.35 V), except for the temperature of the deposition bath, T_{dep}, that was increased from 25, to 50 and to 75 °C for samples NW1, NW2 and NW3, respectively. As seen in Figure 5A, the $I_{max}(200)/I_{max}(220)$ ratio of these deposits decreases steadily from 2.12 ± 0.02 to 1.81 ± 0.02 as T_{dep} is increased from 25 to 75 °C. Therefore, decreasing the electrolyte temperature has a beneficial effect on the orientation of the deposit.

(iii) Effect of the AAO membrane: The effect of the AAO membrane on the preparation of highly-oriented {100} Pt deposit was assessed by performing electrodeposition in the absence of the AAO membrane. For this series of measurements, the conditions that yield the largest $I_{max}(200)/I_{max}(220)$ ratio were chosen (1 mM of Na_2PtCl_6; 100 mM KCl; 10 mM HCl; E_{dep} = –0.35V, T_{dep} = 25 °C). As expected, the absence of the AAO membrane in front of the Ti substrate yields the preparation of the thin film (TF2) whose structure will be examined later. The $I_{max}(200)/I_{max}(220)$ ratio of TF2 is ca. 1.85 ± 0.02, lower than the value of ca. 2.12 ± 0.02 found for NW1 prepared in the same conditions, but with an AAO membrane in front of the Ti substrate. Thus, even if the {100} preferential orientation is less marked for the Pt thin film as compared to the Pt nanowires, a significant {100} preferential orientation is also obtained for Pt deposited in the form of a thin film.

(iv) Effect of the Pt salt concentration: The Pt salt concentrations were varied from 0.25 to 1.00 and to 2.50 mM while all other deposition parameters were kept constant (100 mM KCl; 10 mM HCl; T_{dep}=25 °C; E_{dep}=–0.35 V, no AAO membrane). In this series of measurements, the AAO membrane was omitted and Pt was deposited in the form of a thin film (TF1, TF2 and TF3 for 0.25, 1.00 and 2.50 mM Pt salt concentrations, respectively). As seen in Figure 5B, the $I_{max}(200)/I_{max}(220)$ ratio decreases steadily from 1.92 ± 0.02 to 1.77 ± 0.02 as the Na_2PtCl_6 concentration is increased from 0.25 mM to 2.5 mM, indicating that the {100} preferential orientation of Pt can be enhanced by decreasing the Pt salt concentration in the plating bath.

(v) Effect of the substrate: The deposition of Pt was performed on Ti and carbon cloth substrates using the experimental conditions that yield highly-oriented {100} Pt surfaces (1mM Na_2PtCl_6; 10mM HCl; 100mM KCl; T_{dep} = 25 °C; E_{dep} = –0.35V, no AAO membrane). The diffraction peaks of the carbon cloth substrate interferes with those of the FCC phase of platinum and it was not possible to rely on a measure of the $I_{max}(200)/I_{max}(220)$ ratio to assess the degree of orientation achieved on these two substrates. However, the CVs of both deposits recorded at 5 $mV.s^{-1}$ in 0.5M H_2SO_4 are superimposable on each other (not shown), indicating that the same degree of {100} orientation can be achieved on both substrates. As far as we can tell, the formation of highly-oriented {100} Pt is not dependent on the nature and geometry of the substrate.

2.4. Morphological Characterization

Scanning electron microscopy (SEM) micrographs of various Pt deposits are shown in **Figure 6**. The Pt deposits were prepared in deposition conditions which produced highly {100} oriented (Figure 6A and Figure 6C, corresponding to samples NW2 and TF2, respectively) and non-oriented polycrystalline deposits (Figure 6B and Figure 6D, corresponding to samples NW5 and TF3, respectively). The morphological differences between highly-oriented {100} and polycrystalline Pt deposits are striking. In the case of highly-oriented {100}, the SEM micrographs reveal that both types of deposit (NW and TF) consist of small crystallites with very sharp edges. The insert to Figure 6C (higher magnification) reveals that these crystallites have a pine tree-like structure made of distinct branches which overlap each other. By contrast, such small crystallites with sharp edges are not seen on NW and TF formed in the conditions giving rise to polycrystalline Pt.

Low magnification transmission electron microscopy observations of pine tree-like structures support the low-resolution imaging from the SEM but demonstrate, in addition, highly parallel growth facets on each one of the visible branches (**Figure 7**A). The branches of one single pine tree-like structure are parallel to each other (Figure 7A) and present highly crystalline lattice (Figure 7B) with planes parallel to each other even on adjacent branches (Figure 7C). This indicates that the pine tree-like structure is effectively single crystals. Higher-resolution imaging shows that the growth facets appear to be close to the {100} plane (Figure 7D) which suggests that the growth occurs through the motion of steps on the {100} type plane. This observation also clearly indicates that the plane exposed during the CV experiment is also {100}.

A review of the literature is helpful in understanding the effects of the deposition parameters on the structure of the Pt deposit and how they affect the formation of preferentially-oriented {100} Pt surfaces. There have been many reports in the literature dealing with the preparation of Pt cubic

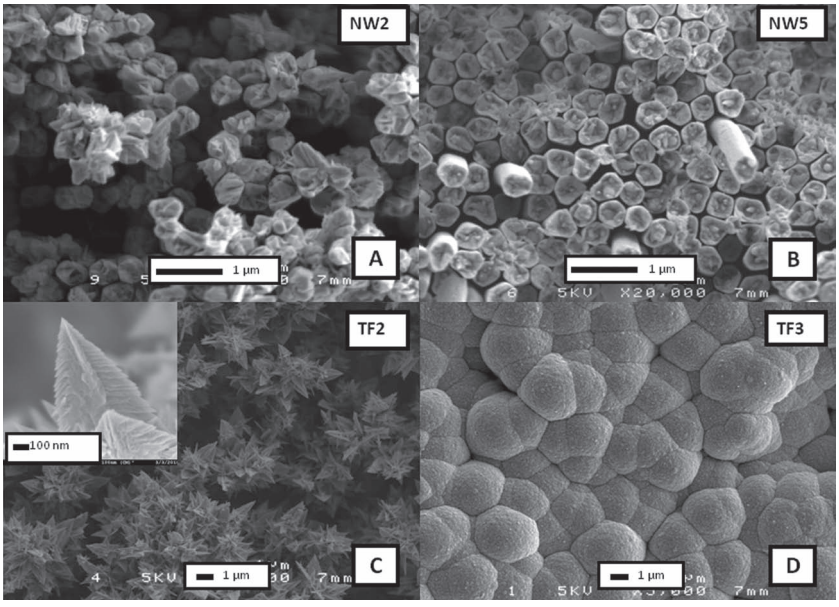

Figure 6. SEM micrographs of Pt nanowires (A and B, corresponding to samples NW2 and NW5, respectively) and Pt thin films (C and D, corresponding to samples TF2 and TF3, respectively). In (A) and (C), the deposition conditions (1 mM Na_2PtCl_6, 10mM HCl, 100 mM KCl, T_{dep} = 25 °C and E_{dep} = –0.35 V) are such that highly-oriented {100} Pt deposits are formed. In (B) and (D), the deposition conditions are such that the structure of the deposit is closer to polycrystalline Pt. The insert shows a high magnification micrograph of TF2. The R_f values of NW2, NW5, TF2 and TF3 are 365, 1016, 666 and 411, respectively.

particles showing a preferential orientation of their surface along the (100) axis. They are synthesized in the form of colloidal platinum, using a capping agent (sodium polyacrylate) and hydrogen gas as a reducing agent. It was shown that the sizes and shapes of the Pt particles were controlled by changes in the ratio concentration of the capping polymer material to the concentration of the Pt cations used.[13] According to high-resolution transmission electron microscopy (HRTEM), these nanoparticles show flat surfaces with {100} facets, and the distances between the adjacent lattice fringes are the interplanar distance of Pt {200}.[14] Pt nanoparticles prepared by the same method have been shown elsewhere to exhibit the characteristic hydrogen adsorption/desorption peaks,[12,15–19] CO-stripping peaks,[17] as well as the characteristic response of irreversibly-adsorbed germanium on (100) terraces of platinum.[18,19] The mechanisms responsible for this effect were identified[32] and are related to the preferential growth of facets due to the adsorption of an organic compound ("capping compound"). As described in the experimental section, no capping agent was used in this study, and the mechanisms responsible for the formation of thin films and nanowires with preferentially-oriented {100} surfaces do not involve the adsorption of an organic compound.

In proton exchange membrane fuel cells, soluble Pt species are reduced by hydrogen permeating from the anode to the cathode side. Ferreira and Shao-Horn have recently shown that the morphology of Pt nanoparticles changed from dentritic shapes to truncated tetrahedrons, truncated octahedrons, and truncated square cuboids as we move away from the carbon support and closer to the membrane-cathode interface.[33] Of special interest to the present study are those Pt nanoparticles with a truncated square cuboid-type shape where {100} Pt planes are predominantly exposed.

The equilibrium shape of an isolated single crystal is determined by the relation $\gamma_i A_i$ = minimum, where γ_i is the surface free energy per unit area A_i of exposed surface (assuming that edge and curvature effects are unimportant). In ideal FCC metals, one would expect the surface free energies to order as $\gamma(111)<\gamma(100)<\gamma(110)$, since surface atom densities are ordered in this manner. This has been confirmed by theoretical studies showing that the surface energy of $\{100\}_{Pt}$ is 190 kJ mol^{-1} per surface Pt atom compared to 153 kJ.mol^{-1} for $\{111\}_{Pt}$.[34] Accordingly, the formation of truncated square cuboid-type shapes with predominantly exposed {100} Pt planes is not expected unless the surface free energies of the crystallographic planes are modified. However, the adsorption of hydrogen at the surface of Pt will modify the surface free energy of the various crystallographic surfaces. As discussed by Markovic and Ross, the enthalpy of H_2 adsorption on the $\{100\}_{Pt}$ is 40–60 kJ.mol^{-1}higher than on the $\{111\}_{Pt}$ surfaces.[35] Accordingly, the surface free energy of $\{100\}_{Pt}$ in the presence of H_2 is lower than $\{111\}_{Pt}$ surfaces and the growth of truncated square cuboid-type shape Pt nanoparticles with predominantly exposed {100} Pt planes is not unexpected in the section of the membrane-electrode assembly closest to the anode of the fuel cell where the concentration of H_2 is higher. Reduction of K_2PtCl_4 using H_2 (without capping polymer) consistently leads to the formation of Pt cubic nanocrystalline particles.[32] By contrast, reduction of H_2PtCl_6 with $NaBH_4$ in ethanol and water[36] or with formic acid[37] results in polycrystalline metallic Pt. All of this suggests that, in the absence of any surfactant or capping agent, reduction of Pt cations in the presence of hydrogen leads to the formation of Pt nanocrystalline particles with highly {100} oriented Pt surfaces, although it must be kept in mind that the change from Pt^{+2} to Pt^{+4} could also be responsible for that variation due to the formation of polycationic Pt precursors in the latter case. Consistently, studies have indicated that the morphology of Pt nanoparticles supported on SiO_2 and γ-Al_2O_3 is influenced by the gaseous species, and that Pt nanoparticles with predominantly {100} (and {110}) surface planes are grown at high temperature in H_2, while all surface crystal planes are formed if they are heated in other gases.[38,39]

Based on the aforementioned considerations, it may be concluded that the presence of hydrogen species (H_2 or H_{ads}) modifies the free surface energy of the various crystallographic surfaces of Pt. Accordingly, the results in Figure 5 may be explained as follows. Electrodeposition of Pt was performed at various electrode potentials (NW2, NW5 and NW4 in Figure 5A). The H_2/H_2O reversible potential is –0.24V *vs* SCE in 0.5M H_2SO_4 solution. Therefore, when deposition is performed at

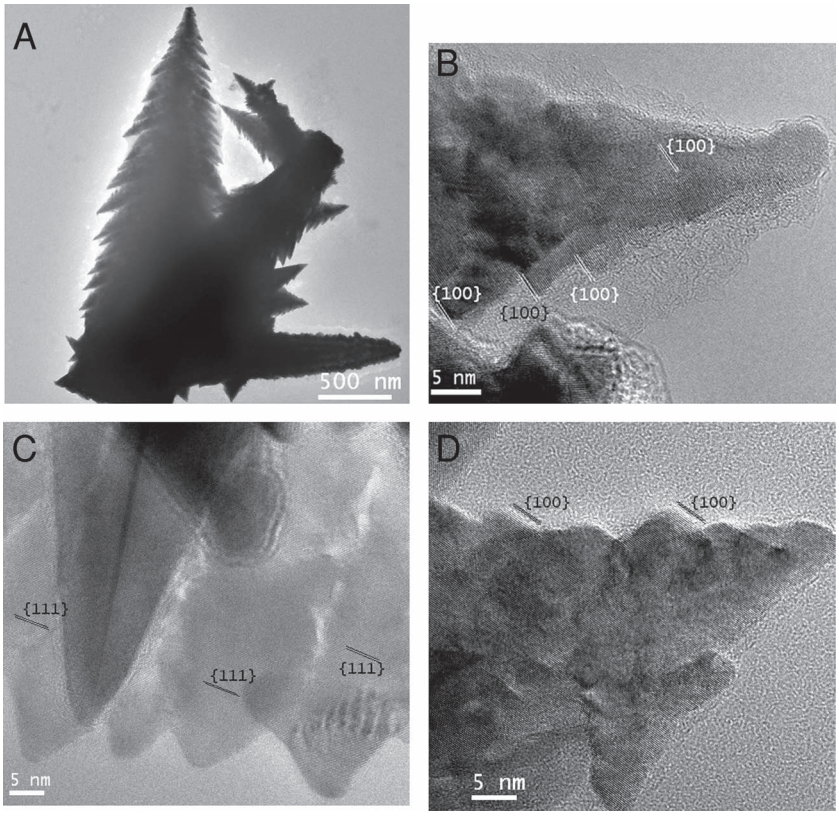

Figure 7. TEM micrographs of the pine-shaped Pt nano structures: (A) low-magnification micrograph, (B) high-resolution image of one of the Pt nanostructure branches highlighting the {100} type steps, (C) high-resolution image of several tips of the Pt nanostructure, demonstrating consistent crystallographic orientation from branch to branch, (D) high-resolution image, again highlighting {100} type steps in the Pt nanostructure.

E_{dep} = –0.35V/ SCE, H_2 is present in the solution and, based on the aforementioned considerations, the formation of a larger fraction of highly-oriented {100} Pt surfaces at E_{dep} = –0.35 V compared to E_{dep} = –0.15 V is expected (hydrogen evolution is not occurring at that potential, and hydrogen adsorption on Pt surfaces is minimal at E_{dep} = –0.15 V *vs* SCE). More surprising is the fact that the fraction of highly-oriented {100} Pt surfaces decreases as the deposition is made more negative (E_{dep} = –0.45V *vs* SCE), despite the fact that hydrogen evolution is more important at more negative potential. This can be understood by considering that the fraction of highly-oriented {100} Pt surfaces decreases as the concentration of Pt^{4+} cations increases in the solution (see Figure 5B). It is hypothesized that stronger hydrogen evolution leads to forced convection in the vicinity of the electrode surface, therefore increasing the concentration of Pt^{4+} cations (see below). Although this effect is not negligible, the fraction of highly {100} oriented Pt surface, as measured by the $I_{max}(200)/I_{max}(220)$ ratio at E_{dep} = –0.45 V, remains higher than at E_{dep} = –0.15 V.

The electrochemical deposition of platinum from hexachloroplatinic acid involves at least two heterogeneous electron transfer processes:[40]

$$[PtCl_6]^{2-} + 2e^- = [PtCl_4]^{2-} + 2Cl^- \; E^0 = 0.485V \; vs \; SCE$$
$$[PtCl_4]^{2-} + 2e^- = Pt + 4Cl^- \; E^0 = 0.517V \; vs \; SCE$$

Films and nanowires were deposited at potentials more negative than *ca.* –0.15 V *vs* SCE. In all cases, the overpotential during the deposition of Pt thin films and nanowires is at least 650 mV. Therefore, it is expected that deposition of metallic Pt is limited by mass transfer (instead of being kinetically limited). According to the Nernst-Planck equation, there are three terms that govern the unidirectional flux of a species *j* to a substrate: (i) migration, (ii) convection, and (iii) diffusion. All the deposits created in this study were made in the presence of a supporting electrolyte ([KCl] = 100 mM). The concentration of the supporting electrolyte exceeds the hexachloroplatinic acid by a factor of one hundred, which means that contribution of migration to the mass-transport of the Pt complex toward the electrode could be neglected. Also, as all deposits were realized in quiescent electrolytes, convection is not expected to play a major role except perhaps in those cases where hydrogen evolution is occurring (for E_{dep} more negative than –0.24 V *vs* SCE), causing unwanted convection of the solution (see above). Therefore, at any given potential, the Pt deposition current is mainly governed by the diffusion of Pt species to the electrode surface, which is thus given by $i = nFD_{Pt}(c_{bulk} - c_{x=0})/\delta$, where these symbols have their usual meaning. Accordingly, the deposition current at any given potential will increase with the hexachloroplatinic acid's bulk concentration, and will decrease as diffusion of the Pt species becomes more sluggish as the temperature of the electrolyte is decreased.

As seen in Figure 5, decreasing the Na_2PtCl_6 salt concentration from 2.50 to 0.25mM and the bath temperature from 75 to 25 °C increases the $I_{max}(200)/I_{max}(220)$.ratio. As shown in the previous discussion, the deposition current is decreased as the concentration of Pt species and temperature of the bath are diminished, which in turn favours the formation of highly-oriented {100} Pt surfaces.

The Pt deposition rate was determined at E_{dep} = –0.35 V, $[Na_2PtCl_6]$ = 0.25 mM and T_{dep} = 25 °C, using an electrochemical quartz crystal microbalance (data not shown). These conditions correspond to TF1 in Figure 5B. The mass varies linearly with time over a period of 8 hours (the measurement was stopped after that). The slope of the mass *vs* time curve is *ca* 5ng.s^{-1}.cm^{-2} or 1.5×10^{13} Pt.atoms.s^{-1}.cm^{-2}. As expected, the Pt deposition rate at E_{dep} = –0.35 V, $[Na_2PtCl_6]$ = 2.50 mM and T_{dep} = 25 °C, which corresponds to the deposition conditions of TF3 in Figure 5B, is 50 ng.s^{-1}.cm^{-2}, ten times larger. These deposition rates correspond to *ca* 1 and 10% of a monolayer per second, respectively. The effect of temperature on the deposition current (and hence on the diffusion coefficient) could not be ascertained, as it was impossible to control the temperature of the EQCM set-up.

From an atomistic viewpoint, the electrodeposition of $PtCl_6^{2-}$ occurs through its transfer from the solution into the ionic metal lattice. The first step of this process is the adsorption

of the Pt species and its subsequent diffusion to a kink site of the {100} oriented Pt surface (it is generally assumed that atoms (ions) are attached to a crystal via a kink site). As may be inferred from the relation between the Pt deposition rate and the proportion of {100} oriented Pt surfaces, the interfacial kinetics of Pt attachment on {100} surfaces of Pt are small. It is hypothesized that diffusion of the Pt species to a kink site must be the rate-limiting step, since the formation of highly-oriented {100} Pt surfaces can be obliterated if the Pt deposition rate is large.

In identical deposition conditions, the presence of an AAO membrane increased the proportion of highly-oriented {100} Pt surfaces (see Figure 5B). This arises because part of the flux of Pt species to the electrode surface is not due to diffusion alone, since hydrogen evolution occurring at that potential (E_{dep} = –0.35V *vs* SCE) is causing a slight convective movement in the electrolyte. Under our experimental conditions, the diffusion layer thickness, δ_0, is ~5 mm larger ($C_0^* = 1 \times 10^{-6}$mole.cm^{-3}, $D_0 = 2.5 \times 10^{-11}$mole.s^{-1}.cm^2, i/nFA = 2.5×10^{-11}mole.s^{-1}.cm^2), than the thickness of the AAO membrane (typically ~60 μm), it is hypothesized that the effective concentration gradient is lower when deposition is performed in the presence of the AAO membrane, yielding a slower Pt deposition rate. Unfortunately, it was impossible to measure the Pt deposition rate in the presence of the AAO membrane using the EQCM set-up.

The proportion of highly-oriented {100} Pt surfaces depends critically on the sample being removed from the solution immediately after the end of the deposition period and not left in open circuit in the deposition bath. The effect of open-circuit potential on the orientation and morphology of highly-oriented {100} Pt deposit is described in detail in the supplementary material section.

As mentioned in the introduction, several papers from Arvia's group have appeared in the literature describing an electrochemical procedure to obtain Pt electrode surfaces with preferred orientations from bulk polycrystalline platinum. The procedure used to achieve this is based on the use of repetitive potential sweeps at high frequency under carefully-selected potential perturbation conditions.[9–11] It was shown that the anodic and cathodic limits of 1.50 V and 0.05 V/ RHE, respectively, were deemed necessary to enhance the {100} preferential orientation, as it was not observed for lower and higher positive and negative potential limits. It was hypothesized that the formation of {100} facets occurs as a result of the formation of a jelly-like metal atom lattice at the positive limit of the scan, which is able to accommodate preferred orientations. Then, the formation of preferentially-oriented {100} surfaces depends on the presence of H, which occurs when the negative limit of the scan is 0.04 V *vs* RHE. In that case, it was hypothesized that the presence of H-adatoms interacting with the metal lattice likely facilitates the formation of a surface structure with a high contribution of (100)-like sites. When the negative limit of the scan is 0.40 V *vs* RHE, H is not present in the vicinity of the electrode surface and (111)-like surface sites are formed.[9] Surface reconstruction was only observed in the case where repetitive triangular potential sweeps between the upper and the lower potential limit were performed at a relatively high frequency (>1000 V.s^{-1}). However, under these conditions, the roughness factor of the preferentially-oriented {100} Pt surface is low and does not exceed R = 3.[9] Experimental evidence of surface modification,[10,11] and crystalline rearrangements [11] were evidenced through scanning tunneling microscopy and XRD, respectively.

The deposits prepared in this study differ from the previous ones in many ways. First, they do not involve the modification of a pre-existing Pt layer and may be grown on a variety of substrates like Ti and carbon paper (see below). Second, both Pt thin films and nanowires may be prepared with a large proportion of preferentially-oriented {100} surfaces. But perhaps the most interesting aspect of this study is the fact that highly-oriented {100} Pt deposits may be obtained with very high roughness factors. A detailed analysis of how the deposition conditions influence the roughness of the deposits is beyond the scope of this work, and will be described in a forthcoming study. However, typical R_f values of *ca*. 700 and 400 were obtained for the highly-oriented {100} Pt thin film (see Figure 6C) and nanowires (see Figure 6A), respectively. These roughness factors are at least two orders of magnitude larger than those reported by Arvia's group since. As we shall see later, the capacity to form highly-oriented {100} Pt thin film and nanowire with very high roughness factors will prove important for the oxidation of hydrazine and ammonia, two reactions known to be favoured by the presence of {100} surfaces.

2.5. Electro-Oxidation of Hydrazine (acidic solution) and Ammonia (alkaline solution)

The electro-oxidation of hydrazine (N_2H_4) is a surface structure-sensitive reaction,[4] and its reaction rate is higher at Pt (100) surface sites compared to other low Miller Index surface orientation.[5,41] Hence, the formation of porous and highly-oriented {100} Pt surfaces may be of interest as an anode catalyst for Direct Hydrazine Fuel Cells (DHFC).[1,42] As a consequence, the use of preferentially-oriented {100} Pt surfaces is a practical strategy to increase the electrocatalytic activity of platinum electrodes for the electro-oxidation of hydrazine.

In **Figure 8**A, a comparison is made between the CV of polycrystalline and highly-oriented {100} Pt surfaces immersed in 0.5M H_2SO_4 + 10 mM N_2H_4. The primary characteristic feature of these CVs is the presence of a large oxidation peak at *ca*. 0.35V with no reduction peak counterpart during the reverse sweep, which indicates that the oxidation of N_2H_4 occurs as a result of a highly irreversible process that yields the formation of gaseous N_2.

Another typical voltammetric feature of preferentially-oriented Pt electrode is the presence of a quasi-reversible oxidation/reduction peak at *ca*. 0.20V. As demonstrated earlier, this peak is related to the oxidative adsorption of hydrazine at low potentials, and is observed only on Pt (100) single crystal surfaces.[4] There is a significant negative shift of the oxidation peak current potential (E_p) from 0.38V (polycrystalline) to 0.32V (highly-oriented {100}). This shift of E_p towards more negative values is attributed to the predominance of {100} microfacets at the surface of the highly-oriented Pt deposit. It is accompanied by a factor of four difference between the specific activities of these two types of deposit, as measured by the peak current, i_p (expressed as μA.cm$^{-2}{}_{Pt}$).

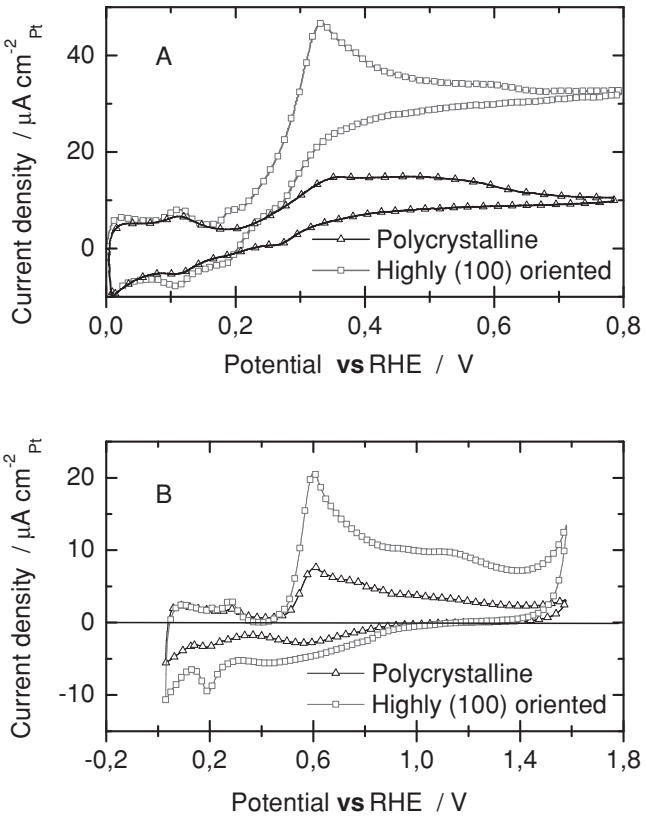

Figure 8. In (A), cyclic voltammogram (5mVs^{-1}) in 0.5 M H_2SO_4 + 10mM N_2H_4 of a polycrystalline and highly-oriented {100} Pt thin films. The roughness factors, R_f, of the polycrystalline and highly-oriented {100} Pt thin films are 200 and 70, respectively. In (B), cyclic voltammogram (5 mVs^{-1}) in 0.1 M NaOH + 10mM NH_3 of a polycrystalline and highly-oriented {100} Pt thin films. The roughness factors, R_f, of the polycrystalline and highly-oriented {100} Pt thin films are 590 and 190, respectively.

The study of the electrochemical behaviour of ammonia is important for environmental electrochemistry (water and air analysis through electrochemical sensors and electrochemical oxidation of ammonia from wastewater streams if the reaction product is N_2 and nitroxides are not formed). More recently, ammonia has attracted attention for the production and storage of hydrogen, and as a possible fuel for direct fuel cells.[1] As shown elsewhere, the oxidation of ammonia on platinum is a surface-sensitive reaction[6,7,8] which takes place almost exclusively on surface sites with (100) symmetry. Consequently, the use of preferentially-oriented {100} Pt surfaces is a practical strategy to increase the electrocatalytic activity of platinum electrodes for the electro-oxidation of ammonia.

In Figure 8B, the oxidation of ammonia in 0.1 M NaOH was performed on polycrystalline and highly-oriented {100} porous Pt electrodes. The electrocatalytic activity of highly-oriented {100} Pt, as given by the normalized current density expressed in μA cm$^{-2}_{Pt,}$ is increased by a factor of 2.7 as compared to polycrystalline platinum electrode, emphasizing the fact that not all Pt atoms on the surface of the deposit are equivalent.

3. Conclusion

It was shown that porous (roughness factors of several hundreds) and highly-oriented {100} Pt thin films and nanowires might be grown on the surface of Ti and carbon paper substrates. The occurrence of {100} facets on the surface of the deposit is critically dependent on the presence of hydrogen during the electrodeposition of Pt. It is hypothesized that the surface free energy of $\{100\}_{Pt}$ in the presence of H_2 is lower than $\{111\}_{Pt}$ surfaces. In these conditions, the growth of predominantly exposed {100} Pt planes is expected. The interfacial kinetics of Pt attachment on {100} surface are low, and highly-oriented Pt thin films and nanowires are obtained only by reducing the deposition rate of Pt, which is achieved by lowering the Na_2PtCl_6 salt concentration and the temperature of the electrolyte. The mechanisms responsible for the deposition of {100} oriented Pt surface is not dependent on the nature of the substrate and highly oriented Pt thin films could be prepared on dense Ti and porous carbon substrates. Due to the predominance of {100} facets, electrodes made of highly-oriented Pt surfaces exhibit improved electrocatalytic activity for the oxidation of hydrazine (in acidic electrolyte) and ammonia (in alkaline electrolyte). This is consistent with the well-established fact that the electro-oxidation of small nitrogen hydride molecules such as hydrazine and ammonia is structure-sensitive, with the {100} planes being the most active.

4. Experimental Section

Pt thin films (TFs) and Pt nanowires (NWs) were electroplated on Ti substrates (1 cm^2) and the experimental setup for the preparation of Pt TFs and NWs was described elsewhere.[43,44] Details are given in the supplementary section. The working electrode was a Ti plate while Pt gauze was used as counter electrode. A saturated calomel electrode was used as reference electrode. A Luggin capillary was employed to minimize the iR drop. All samples were thoroughly rinsed with water after plating. Pt deposits were also performed onto carbon substrates (carbon paper, Spectracorp, 2050-A0850).

The deposits were prepared by potentiostatic electrodeposition using acidified (HCl) $Na_2PtCl_6.xH_2O$ solutions, with KCl as supporting electrolyte. The deposition potential (E_{dep}), the temperature of the bath during deposition (T_{dep}), and the $Na_2PtCl_6.xH_2O$ concentration were systematically varied. The concentrations of HCl (10 mM) and KCl (100 mM) were kept constant for all experiments.

The surface morphology of the deposits was examined by scanning electron microscopy (SEM) on a JEOL JSM-6300 microscope at an accelerating voltage of 5kV. The crystallographic structures were analyzed by X-ray diffraction (XRD) measurements on a Bruker D8 Advanced X-ray diffractometer with Cu K_α radiation (1.54184 Å), operating at 40 kV and 40 mA. High-resolution transmission electron microscopy (TEM) was carried out on a FEI Titan 80–300 TEM equipped with an aberration corrector for the imaging lens (CEOS). The material was scraped from the substrate and suspended in water. A drop of solution was put on a holey carbon film supported by a Cu grid and left to dry before being inserted in the TEM.

The electrochemical measurements were carried out in a three-compartment cell at room temperature with platinum gauze and a Reversible Hydrogen Electrode (RHE) as auxiliary and reference electrodes, respectively. Cyclic voltammograms were recorded in de-aerated (Argon N5.0, Praxair) 0.5M ultrapure sulphuric acid (A300-212, Fisher Scientific). The electrode potential was first cycled at 50 mVs^{-1} up to 0.8 V until a stationary voltammetric profile was obtained. All current densities are

normalized to the true surface area of Pt determined from the hydrogen desorption charge. All cyclic voltammograms have been corrected for the uncompensated ohmic drop. Gold-plated crystals (9 MHz AT-cut) were used for the electrochemical quartz crystal microbalance (EQCM) experiments. The Pt deposition rates were determined as described elsewhere.[29]

Supporting Information

Supporting Information is available from the Wiley Online Library or from the author.

Acknowledgements

This work was supported by the Natural Sciences and Engineering Research Council of Canada (NSERC), the Canada Research Chair program, the Fonds Québécois de la Recherche sur la Nature et les Technologies (FQRNT) and the NSERC Hydrogen Canada (H2CAN) Strategic Research Network, for supporting this work. Transmission electron microscopy was carried out at the Canadian Centre for Electron Microscopy, a facility supported by NSERC and McMaster University. Also, one of us (EB) would like to acknowledge the financial support of NSERC through an Alexander Graham Bell Canada Graduate Scholarship (CGS) (Masters Degree) and the Fonds québécois de la recherche sur la nature et les technologies (FQRNT) through the master research scholarships (B1) program.

Received: February 7, 2012
Revised: April 7, 2012
Published online: June 14, 2012

[1] N. V. Rees, R. G. Compton, *Energy Environ. Sci.* **2011**, *4*, 1255.
[2] C. Nishihara, I. A. Raspini, H. Kondoh, H. Shindo, M. Kaise, H. Nozoye, *J. Electroanal. Chem.* **1992**, *338*, 299.
[3] R. Gomez, J. M. Orts, A. Rodes, J. M. Feliu, A. Aldaz, *J. Electroanal. Chem.* **1993**, *358*, 287.
[4] B. Alvarez-Ruiz, R. Gomez, J. M. Orts, J.M. Feliu, *J. Electrochem. Soc.* **2002**, *149*, D35.
[5] V. Rosca, M. T. M. Koper, *Electrochim. Acta* **2008**, *53*, 5199.
[6] F. J. Vidal-Iglesias, N. Garcıa-Araez, V. Montiel, J. M. Feliu, A. Aldaz, *Electrochem. Commun.* **2003**, *5*, 22.
[7] F. J. Vidal-Iglesias, J. Solla-Gullon, V. Montiel, J. M. Feliu, A. Aldaz, *J. Phys. Chem. B* **2005**, *109*, 12914.
[8] V. Rosca, M. T. M. Koper, *Phys. Chem. Chem. Phys.* **2006**, *8*, 2513.
[9] R. M. Cervino, W. E. Triaca, A. J. Arvia, *J. Electroanal. Chem.* **1985**, *182*, 51.
[10] J. Gomez, L. Vazquez, A. M. Baro, N. Garcia, C. L. Perdriel, W. E. Triaca, A. J. Arvia, *Nature* **1986**, *323*, 612.
[11] W. E. Triaca, A. J. Arvia, *J. Appl. Electrochem.* **1990**, *20*, 347.
[12] F. J. Vidal-Iglesias, J. Solla-Gullon, V. Montiel, J. M. Feliu, A. Aldaz, *J. Power Sources* **2007**, *171*, 448.
[13] T. S. Ahmadi, Z. L. Wang, T. C. Green, A. Hengleina, M. A. El-Sayed, *Science* **1996**, *272*, 1924.
[14] T. S. Ahmadi, Z. L. Wang, A. Henglein, M. A. El-Sayed, *Chem. Mater.* **1996**, *8*, 1161.
[15] S. Brimaud, S. Pronier, C. Coutanceau, J. M. Léger, *Electrochem. Commun.* **2008**, *10*, 1703.
[16] P. Urchaga, S. Baranton, T. W. Napporn, C. Coutanceau, *Electrocatalysis* **2010**, *1*, 3.
[17] P. Urchaga, S. Baranton, C. Coutanceau, G. Jerkiewicz, *Langmuir* **2012**, *28*, 3658.
[18] P. Rodriguez, E. Herrero, J. Solla-Gullon, F. J. Vidal-Iglesias, A. Aldaz, J. M. Feliu, *Electrochim. Acta* **2005**, *50*, 4308.
[19] J. Solla-Gullon, P. Rodriguez, E. Herrero, A. Aldaz, J. M. Feliu, *Phys. Chem. Chem. Phys.* **2008**, *10*, 1359.
[20] J. Solla-Gullon, V. Montiel, A. Aldaz, J. Clavilier, *J. Electroanal. Chem.* *491*, 69.
[21] L. Y. Zhao, A. C. Siu, L. J. Pariag, Z. H. He, K. T. Leung, *J. Phys. Chem Lett.*, **2007**, **111**, 14621–14624.
[22] N. Tian, Z. Y. Zhou, N. F. Yu, L. Y. Wang, S. G. Sun, *J. Am. Chem. Soc.* **2010**, *132*, 7580.
[23] S. Garbarino, A. Ponrouch, S. Pronovost, J. Gaudet, D. Guay, *Electrochem. Commun.* **2009**, *11*, 1924.
[24] J. Solla-Gullon, F. J. Vidal-Iglesias, P. Rodriguez, E. Herrero, J. M. Feliu, J. Clavilier, A. Aldaz, *J. Phys. Chem. C* **2004**, *108*, 13573.
[25] D. J. Jenkins, A. M. S. Alabdulrahman, G. A. Attard, K. G. Griffin, P. Johnston, P. B. Wells, *J. Catalysis* **2005**, *234*, 230.
[26] I. Bakos, G. Horanyi, *J. Electroanal. Chem.* **1992**, *332*, 147.
[27] I. Bakos, G. Horanyi, *J. Electroanal. Chem.* **1995**, *397*, 105.
[28] P. Rodrıguez, J. Solla-Gullon, F. J. Vidal-Iglesias, E. Herrero, A. Aldaz, J. M. Feliu, *Anal. Chem.* **2005**, *77*, 5317.
[29] A. Ponrouch, S. Garbarino, S. Pronovost, P. L. Taberna, P. Simon, D. Guay, *J. Electrochem. Soc.* **2010**, *157*, K59.
[30] A. Ponrouch, S. Garbarino, D. Guay, *Electrochem. Commun.* **2009**, *11*, 834.
[31] S. Garbarino, A. Ponrouch, S. Pronovost, D. Guay, *Electrochem. Commun.* **2009**, *11*, 1449.
[32] J. M. Petroski, Z. L. Wang, T. C. Green, M. A. El-Sayed, *J. Phys. Chem. B* **1998**, *102*, 3316.
[33] P. J. Ferreira, Y. Shao-Horn, *Electrochem. Solid-State Lett.* **2007**, *10*, B60.
[34] S. M. Foiles, M. I. Baskes, M. S. Daw, *Phys. Rev. B* **1986**, *33*, 7983.
[35] N. M. Markovic, P. N. Ross, *Surf. Sci. Rep.* **2002**, *45*, 117.
[36] H. Zhou, W.P. Zhou, R. R. Adzic, S. S. Wong, *J. Phys. Chem. C* **2009**, *113*, 5460.
[37] S. Sun, D. Yang, D. Villers, G. Zhang, E. Sacher, J.P. Dodelet, *Adv. Mater.* **2008**, *20*, 571.
[38] T. Wang, C. Lee, L. D. Schmidt, *Surf. Sci.* **1985**, *163*, 181.
[39] K. Hayek, *J. Mol. Catal.* **1989**, *51*, 347.
[40] F. Colom, in *Standard Potentials in Aqueous Solutions* (Eds: A. J. Bard, R. Parsons, J. Jordan), Marcel Dekker, New York **1985**, p. 339.
[41] M. D. Garcia Azorero, M. L. Marcos, J. Gonzalez Velasco, *Electrochim. Acta* **1994**, *39*, 1909.
[42] K. Asazawa, K. Yamada, H. Tanaka, A. Oka, M. Taniguchi, T. Kobayashi, *Angew. Chem. Int. Ed.* **2007**, *46*, 8024.
[43] P. L. Taberna, S. Mitra, P. Poizot, P. Simon, J. M. Tarascon, *Nat. Mater.* **2006**, *5*, 567.
[44] A. Ponrouch, M.P. Bichat, S. Garbarino, C. Maunders, G. Botton, P.L. Taberna, P. Simon, D. Guay, *ECS Trans.* **2010**, *25*, 3.